Three-dimensional Finite-element Forward Modeling of Electromagentic Data using Potentials and Unstructured Meshes

SeyedMasoud Ansari and Colin G. Farquharson

Department of Earth Sciences, Memorial University of Newfoundland, St. John's , Canada

SEG LasVegas 2012

Society of Exploration Geophysics
82nd Annual Meeting
Mandalay Bay Convention Center
4-9 November, Las Vegas, NV, USA

Introduction and Motivation

Forward Modeling

Definition:

What a sensor (A loop of current for example) would measure if the actual formation of the subsurface matches a given model.

Purpose:

In order to extract as much information as possible from survey data forward modeling for complex 3D Earth models are required.

Structured Vs. Unstructured Grids

Unstructured grids provide more flexibility in generating the complex-shaped Earth geometries such as curved objects (see Figure 2 -b) and topography features. Furthermore from the computational standpoint, the ability to locally refining the mesh at the regions of interest and coarsening it near the truncation boundaries (see Figure 2 - d) is a particular benefit of using unstructured meshes. In fact, this could be an advantage over the structured rectangular grids (see Figure 2 - c) where having small cells close to the boundaries of the mesh is inevitable and results in computational inefficiencies.

Inductive and Galvanic parts

Despite the long history of EM methods in geophysical exploration, there has not yet been a thorough investigation of the inductive and galvanic effects and interplay between them. Induction is characterized by coupling via a time varying magnetic field, both between a closed-loop transmitter and an isolated conductor. By contrast, a synopsis of the galvanic process would be the direct flow of the current to and from the grounded source similar to what is observed in DC resistivity methods. In fact, channelling of the current at the regions of conductivity gradient characterizes the galvanic response.

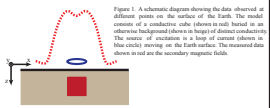

Figure 1. A schematic diagram showing the data observed at different points on the surface of the Earth. The model consists of a conductive cube (shown in red) buried in an otherwise background (shown in beige) of distinct conductivity. The source of excitation is a loop of current (shown in blue circle) moving on the Earth surface. The measured data shown in red are the secondary magnetic fields.

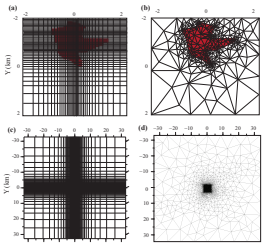

Figure 2. Generating the curved underground body using (a) structured rectilinear and (b) unstructured tetrahedral grids. An entire view of the mesh subdivided into (c) structured and (d) unstructured elements.

Methodology

E-field Equation:

In the quasi-static regime the electric field satisfies the following equation:

$$\nabla \times \nabla \times \mathbf{E} + i\omega\mu_0\sigma\mathbf{E} = -i\omega\mu_0\mathbf{J}^s$$

where $\mathbf{E}$ is the electric field, μ_0 is the magnetic permeability of free space, σ is the electrical conductivity, and $\mathbf{J}^s$ is the current density of the source.

Decomposition:

In our formulation the electric field is decomposed into vector magnetic potential, $\mathbf{A}$, (scaled by $-i\omega$) and scalar electric potential, ϕ :

$$\mathbf{E} = -i\omega\mathbf{A} - \nabla\phi.$$

Equations to be Discretized:

$$\nabla \times \nabla \times \mathbf{A} + i\omega\mu_0\sigma\mathbf{A} + \mu_0\sigma\nabla\phi = \mu_0\mathbf{J}^s$$

$$-i\omega\nabla \cdot (\sigma\mathbf{A}) - \nabla \cdot (\sigma\nabla\phi) = -\nabla \cdot \mathbf{J}^s$$

Finite-Element method:

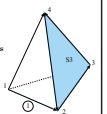

Figure3. A typical tetrahedral element. Four nodes and six edges are shown for this element.

$$\mathbf{A} = \sum_{j=1}^{N_{edges}} \tilde{A}_j \, \mathbf{N}_j \qquad \phi = \sum_{k=1}^{N_{nodes}} \tilde{\phi}_k \, N_k$$

where $\tilde{A}_j$ and $\tilde{\phi}_k$ are the approximated vector and scalar potentials. $\mathbf{N}_j$ and N_k are also the edge-element and the nodal-element basis functions in each tetrahedron.

The System of Equations Solved:

$$\begin{pmatrix} \mathbf{C} & -\omega\mu\mathbf{D} & \mu\mathbf{F} & 0 \\ \omega\mu\mathbf{D} & \mathbf{C} & 0 & \mu\mathbf{F} \\ 0 & -\omega\mathbf{F}^{\mathbf{T}} & \mathbf{H} & 0 \\ \omega\mathbf{F}^{\mathbf{T}} & 0 & 0 & \mathbf{H} \end{pmatrix} \begin{pmatrix} \tilde{A}^R \\ \tilde{A}^I \\ \tilde{\phi}^R \\ \tilde{\phi}^I \end{pmatrix} = \begin{pmatrix} \mu S_1 \\ 0 \\ S_2 \\ 0 \end{pmatrix}$$

where $C_{ij} = \int_\Omega (\nabla \times \mathbf{N}_i) \cdot (\nabla \times \mathbf{N}_j) \, d\Omega$

$D_{ij} = \int_\Omega \sigma \, \mathbf{N}_i \cdot \mathbf{N}_j \, d\Omega$

$H_{ik} = \int_\Omega \nabla N_i \cdot (\sigma \, \nabla N_k) \, d\Omega$ with $i, j = 1, \cdots, N_{edges}$ and $l, k = 1, \cdots, N_{nodes}$

$F_{il} = \int_\Omega \nabla N_i \cdot (\sigma \, \mathbf{N}_j) \, d\Omega$

$\mathbf{F}^{\mathbf{T}}$ is the transpose of the matrix $\mathbf{F}$

$\tilde{A}^R$ and $\tilde{A}^I$ are real and imaginary parts of the approximated vector potential

$\tilde{\phi}^R$, and $\tilde{\phi}^I$ are real and imaginary parts of the approximated scalar potential

Verifications and Examples

1 - Controlled-source Electromagnetics (CSEM):

1 - 1 Horizontal Electric Dipole source (HED) for a half-space model

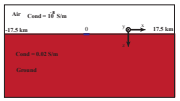

Figure 4. a) The 3D geometry of the half-space model. The 1 meter electric dipole source is located on the air-ground interface.

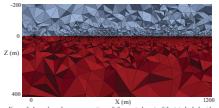

Figure 5. An enlarged xz cross-section of the central part of the tetrahedral grid used for the homogeneous half-space model. The conductive ground and the resistive air are shown in red and blue respectively. The Earth surface is flat and the mesh is refined about the dipole source at the origin (X = 0 and Z = 0) and along 1000 meters of observation locations.

The Quality mesh is generated using the **TetGen** Library (Si, 2007) which does a delaunay small tetrahedralization of the entire computational domain. The dimension of the whole mesh is 35 km×35 km×35 km. The respective number of nodes and edges for are **16907** and **117673** which leads to **273160** of unknowns for the vector and scalar potentials together. The resulting system is solved using the iterative solver of **GMRES** (Generalized Minimum Residual) from **SPARSKIT** (Saad, 1990) with a preconditioning of the coefficient matrix. Here after about **1600** iterations a residual norm of 10^{-7} was reached.We also chose a fill-in parameter of **lfil = 3** for the **ILUT** preconditioner. The dimension of the **Krylov subspace** was also set to **100** for this run.

Electric Fields Computed : x- component of the electric field and the residual norm are shown below.

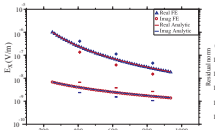

Figure 6. The x component of the electric field for a frequency of 3 Hz. The blue triangle and red circles are the real and imaginary parts of the electric field calculated using the finite-element method. The red and blue solid lines are also the real and imaginary parts of the electric field calculated using the analytic formula given by Ward and Hohmann (1988)

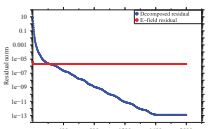

Figure 7. The convergence for the E-field and decomposed solutions for a frequency of 3 Hz. The respective red and blue curves are the residual norm for the E-field and the decomposed find solutions.

Inductive and Galvanic Components :

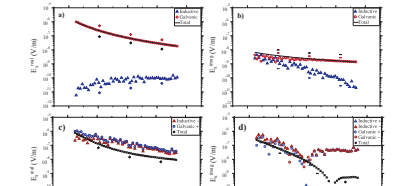

Figure 8. The inductive and galvanic parts of the electric field for frequencies of 3 Hz and 300 Hz for a conductive half-space model of 0.02 S/m. Positive and negative symbols are for the signs of the fields. For 3 Hz the inductive and galvanic components of the the a) real and the b) imaginary parts of the electric field are shown respectively. For 300 Hz the inductive and galvanic components of the the e) real and the d) imaginary parts of the electric field are shown respectively.

1 - 2 Long Grounded Wire source for a prism in a half-space model

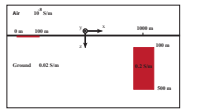

Figure 9. The 3D geometry of the prism model. The **100 meters** grounded wire source is located on the air-ground interface. The dimension of the conductive prism is **120 - 200 - 400** in the x-, y-, and z- directions

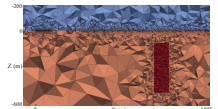

Figure 10. An enlarged xz cross-section of the central part of the tetrahedral grid. The conductive ground and the resistive air are shown in light brown and blue respectively. The conductive prism is also shown in red. The mesh is refined about the grounded wire and 1000 meters of observation locations.

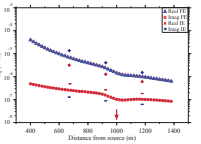

Figure 11. The x component of the electric field for a frequency of 3 Hz. The blue triangles and red circles are the real and imaginary parts of the electric field calculated using the FE method. The red and blue crosses are also the real and imaginary parts of the field calculated using Integral-Equation of **Farquharson and Oldenburg (2002)**. The location of the body is shown using the red arrow.

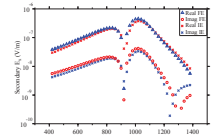

Figure 12. A comparison for the real and imaginary parts of the secondary electric field computed using the finite-element (blue triangles and red circles) and the integral-equation method (red and blue crosses).

Inductive and Galvanic Components :

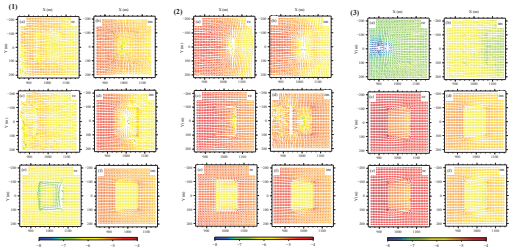

Figure 13. Arrows of the inductive part, the galvanic part and the total electric field for the prism in the half-space model. Fields are shown for three frequencies: (1) **1000** Hz, (2) **150** Hz, and (3) **3** Hz. For each frequency all six panels show the horizontal component of the fields at a depth of 150 m in the ground. Direction and strength of the fields are characterized using arrows and colors. The real (a), and the imaginary (b) components of the inductive part; the real(c), and the imaginary (d) component of the galvanic part, and the real (e), and the imaginary (f) component of the total field are shown.

Contact : SeyedMasoud Ansari at seyedmasoud.ansari@mun.ca
Colin Farquharson at cgfarquh@mun.ca

2 - Transmitter-Receiver pair for a Large Conductivity Contrast

The algorithm is also verified for a model containing a large conductivity contrast. The conductivity ratio of the graphite (shown in red in Figure 14) to the background brine is 8630.13. The transmitter-receiver pair, which are two loop of currents, move at a height of 2 cm above the surface of the brine. Here, in order to strongly prove the correctness of our method a comparison with the **physical scale modeling** (PSM) of **Duckworth and Kerbes** (1997) and **Duckworth et. al.** (2001) is done. The PSM experiment is performed in the labartory.

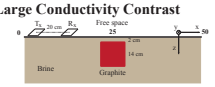

Figure 14. The graphite cube immersed in brine. The conductivity of the graphite and the brine are 61000 S/m and 7.1 S/m respectively. The transmitter-receiver pair is in the free-space and moves at a height of 2 cm above the surface of the brine.

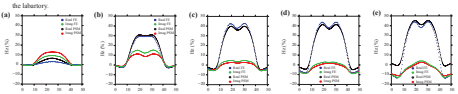

Figure 15. Results for the cube in brine model. The secondary Hz (%), which is the total field minus the free-space a field normalized by the free-space field, is shown for five frequencies: **a)** 1 kHz, **b)** 10 kHz, **c)** 100 kHz, **d)** 200 kHz, e) 400 kHz

Inductive and Galvanic Components :

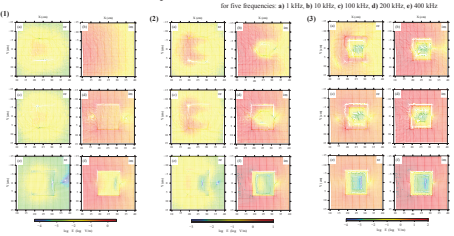

Figure 16. Arrows of the inductive part, the galvanic part and the total electric field for the cube in brine model. Fields are shown for three frequencies: (1) **1** kHz, (2) **10** kHz, and (3) **100** kHz. For each frequency all six panels show the horizontal component of the fields at a depth of 5 cm . Direction and strength of the fields are characterized using arrows and colors. The real (a), and the imaginary (b) components of the inductive part; the real(c), and the imaginary (d) component of the galvanic part, and the real (e), and the imaginary (f) component of the total field are shown. The center of the source-receiver pair is located at x = 25 cm here.

Conclusions

- Unstructured meshes are efficiently used for forward modeling of 3D geophysical electromagnetic problems.
- An **A – φ** decomposition of the electric field leads to a fast solution particularly for lower frequencies.
- The correctness of our algorithm is confirmed for two important geophysical surveys: for the commonly used grounded-wire source and for the moving transmitter-receiver loop.
- Inductive and galvanic component are extracted and the interplay between them for different geophysical scenarios are explored.
- The method presented and the algorithm written here are verified for models containing large conductivity contrasts.

References:

1- Ansari, S. and Farquharson, C., G., 2011, 3D finite-element simulation of electromagnetic data for inductive and galvanic components, SEG Expanded Abstracts, 30, 766.

2- Duckworth, K., and E. S. Kerbes, 1997, The response of steeply dipping tubular conductors located in conductive host rocks when detected by horizontal coplanar coil and vertical coincident coil electromagnetic exploration systems: Canadian Journal of Exploration Geophysics, 33,55-65

3- Duckworth, K., T. D. Nicholas, and E. S. Kerbes, 2001, Examination of the relative influence of current gathering on fixed loop and moving source electromagnetic survey: Geophysics, 66, 1059-1066

4- Farquharson, C. G. and D. W. Oldenburg, 2002, An integral equation solution to the geophysical electromagnetic forward-modelling problem, in M. S. Zhdanov and P. E. Wannamaker, eds., Three-dimensional Electromagnetics: Elsevier, Inc., 3-19

5- Saad, Y., 1990, SPARSKIT: a basic tool kit for sparse matrix computations, Report RIACS-90-20, Research Institute for Advanced Computer Science, NASA, Ames Research Center.

6- Si, H., 2007, TetGen: A quality tetrahedral mesh generator and 3D delaunay triangulator, Weierstrass Institute for Applied Analysis and Stochastics, Berlin, Germany. Available from http://tetgen.berlios.de

7- Ward, S. H., and G. W. Hohmann, 1988, Electromagnetic theory for geophysical applications: in M. N. Nabighian, Electromagnetic methods in applied Geophysics, 1, 131-311